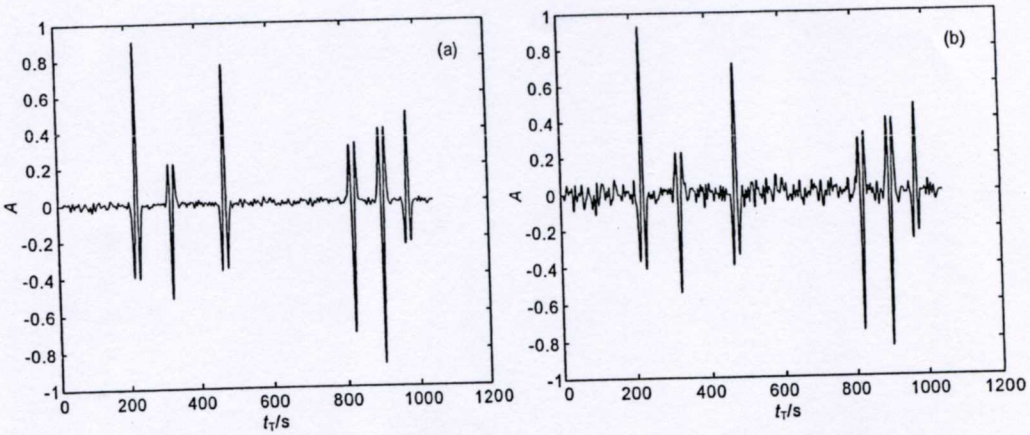

Fig. 3 Regularizing migration results as noise level equal to 0.01 (a) and 0.03)(b)

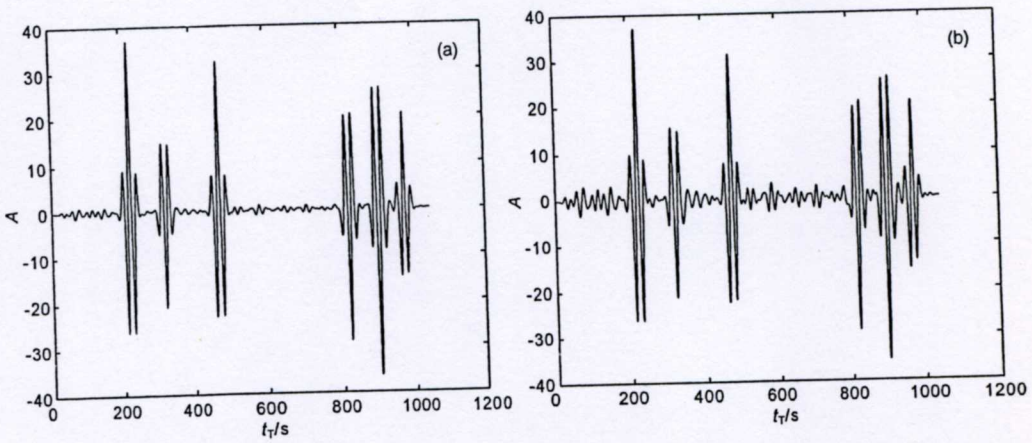

Fig. 4 Kirchhoff migration results as noise level equal to 0.01 (a) and 0.03 (b)

6.2 Two-Dimensional Seismic Migration Deconvolution/Inversion Imaging

The second example is a two-dimensional migration problem. We assume that receivers are uniformly distributed on a line with maximum line length 2501 m. A sampling interval of 40 m in x coordinate is assumed. An impulsive source wavelet that generates 63 traces of seismic data, the background velocity is homogeneous with c=5000 m/s, and the time sampling interval is dt=1.3 m/s. The spatial resolution of the migration inversion image is influenced by the migration inversion filter length in the z-coordinate which defines the number of neighboring depth levels around the given depth. In this simulation, the grid dimensions of the model is 2501×1001 with an x gridpoint spacing of dx=40 m, and a z gridpoint spacing of 12.5 m. The three point scatterers are buried at different depth: 616.5 m, 741.5 m and 866.5 m. We apply our algorithm to the common shot gather for three single shots in the middle of a recording geometry. For a point scatterer, imaging the earth had just one point reflector at (x_0, z_0). This reflector explodes at $t = 0$. The data at z is a function of locations x and travel time t would be an impulsive signal along the hyperbolic trajectory $t^2 = 1/v^2((x-x_0)^2+(z-z_0)^2)$. For different depth z underground, the travel time t would be $t_T = 1/v\sqrt{(x-x_0)^2+(z-z_0)^2}$. The noise level is assumed to be 0.01. The initialization of the our algorithm is as follows: the initial model is chosen as zero, the regularization parameter α is set as 0.005. The regularized migration image and the standard migration image are shown in Figs. 5a and 5b, respectively. It is clear that the regularized migration image possesses better resolution than that of standard migration image.

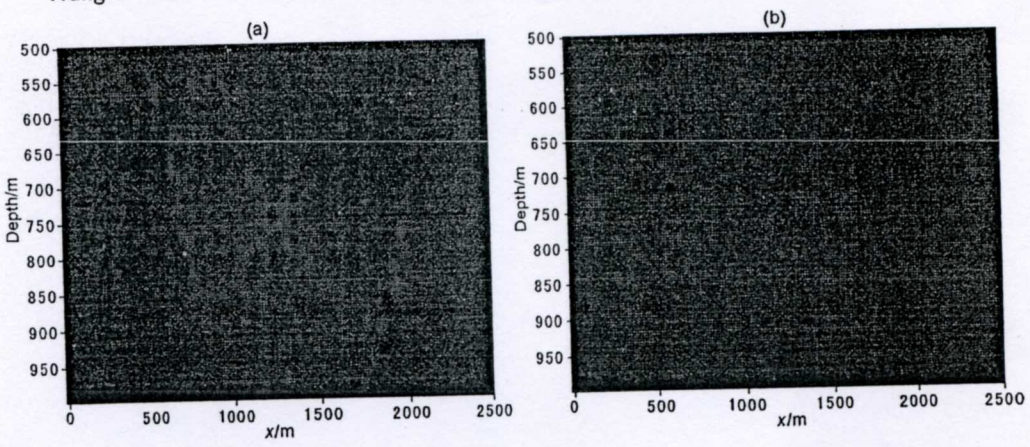

Fig. 5 Standard Kirchhoff migration results (a) and regularized migration image (b)

6.3 Three-Dimensional Seismic Migration Deconvolution/Inversion Imaging

We assume that receivers are uniformly distributed on a 21×21 orthogonal grid with a sampling interval of 40 m in x coordinate and 20 m in y coordinate. An impulsive source wavelet generates 21×21 traces of seismic data, the background velocity is homogeneous with c=5000 m/s, and the time sampling interval is $\mathrm{d}t = 1.7$ ms. The grid dimensions of the model will be $21 \times 21 \times 10$ points with an x or y gridpoint spacing of $\mathrm{d}x = 40$ m, $\mathrm{d}y = 20$ m and a z gridpoint spacing of 200 m. One point scatterer and ten point scatters are used for simulation. Point scatterers are buried at a depth of 1000 ~2800 m. We apply our algorithm to the common shot gather for a single shot in the middle of a recording geometry. In this test, the regularization parameter is chosen as $\alpha = 0.001$. The noise level is assumed to be 0.001.

The standard Kirchhoff migration image and the regularized migration image for one point scatterer model and ten point scatters model are illustrated in Figs. 6~9, respectively. It is apparent that the regularized migration images possess better resolution than that of standard migration image.

We find in computation that, under the same condition, our hybrid gradient method yields higher precision than that of Fletcher-Reeves conjugate gradient method: for one point scatterer model, the norm of the residual for Fletcher-Reeves algorithm in 45 iteration cycles is 0.0476, the CPU cost is 311.2969 s; the norm of the residual for our algorithm in 45 iteration cycles is 0.0345, the CPU cost is 248.8750 s. For ten point scatterers model,

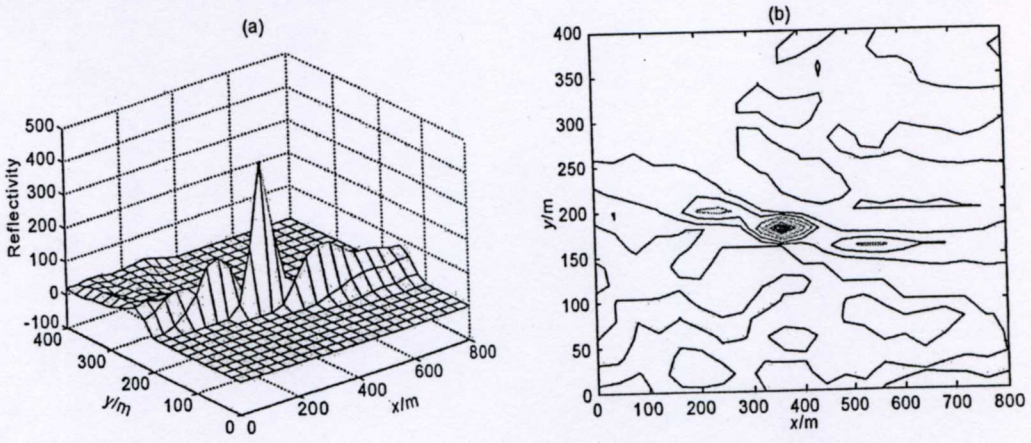

Fig. 6 Standard Kirchhoff migration results for one point scatterer model (a) and contour values of the standard Kirchhoff migration results for one point scatterer model (b)

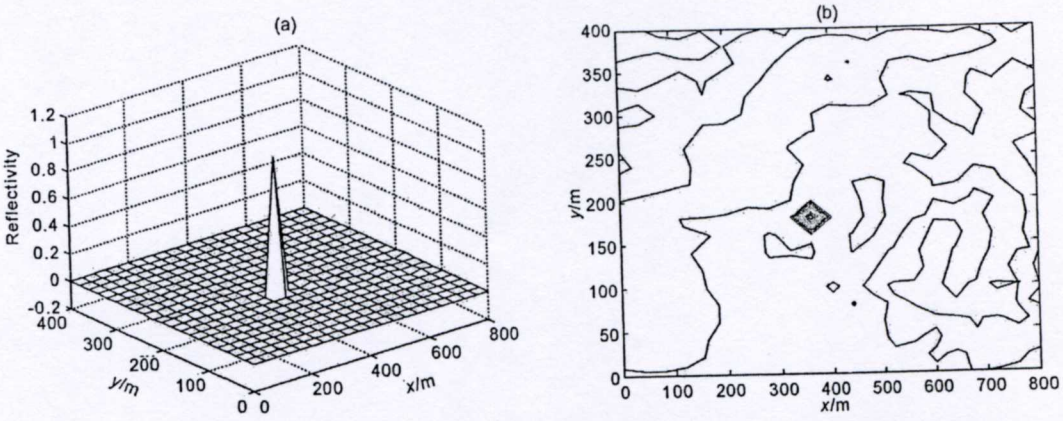

Fig. 7 Regularized migration results for one point scatterer model (a) and contour values of the regularized migration results for one point scatterer model (b)

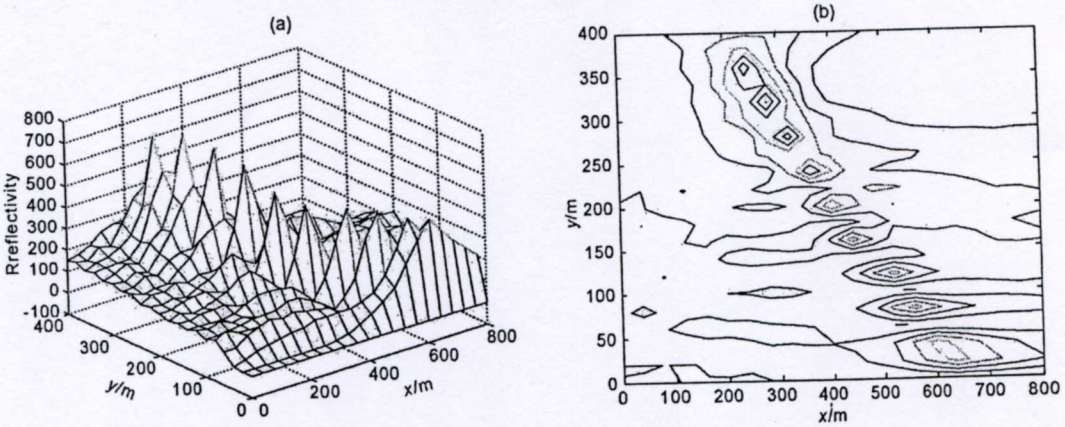

Fig. 8 Standard Kirchhoff migration results for ten point scatterers model (a) and contour values of the standard Kirchhoff migration results for ten point scatterers model (b)

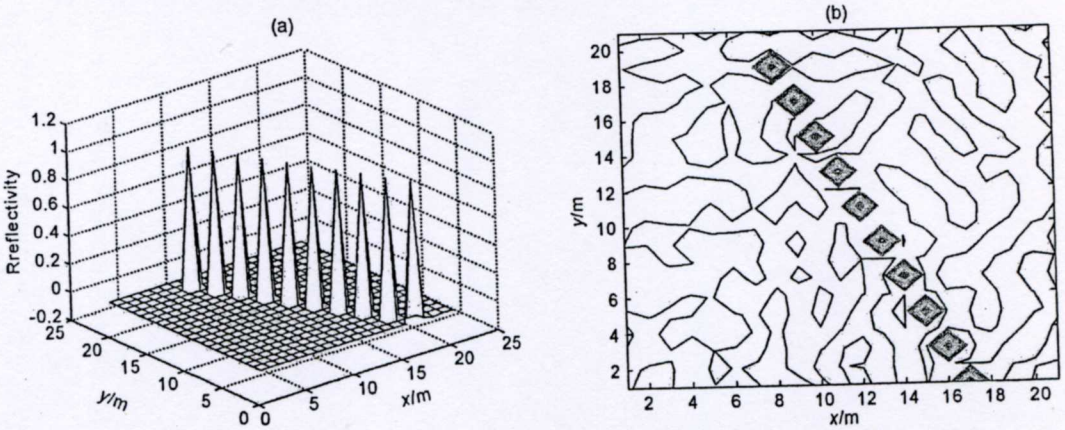

Fig. 9 Regularized migration results for ten point scatterers model (a) and contour values of the regularized migration results for ten point scatterers model (b)

the norm of the residual for Fletcher-Reeves algorithm in 45 iteration cycles is 0.0021, the CPU cost is 253.1406 s; the norm of the residual for our algorithm in 45 iteration cycles is 0.0020, the CPU cost is 248.9063 s.

6.4 Seismic Deconvolution/Inversion Imaging Using Finite Difference Seismogram

In this section, we show that our algorithm is workable for migration deconvolution and inversion imaging for synthetic data using a finite-difference (FD) modeling method. The finite difference seismogram is generated by convolving the source wavelet with a simple 4 layer velocity model and a small channel beneath a layered medium simulating a point scatterer. We perform a 5 point approximation to the acoustic wave equation, and additive Gaussian noise with noise level equaling to 0.01 is added to the seismogram. The recorded seismograms are given in Fig. 10. The standard migration image and the regularized migration image are shown in Figs. 11a and 11b, respectively. Again it shows that the regularized migration deconvolution and inversion yields recovery with better resolution.

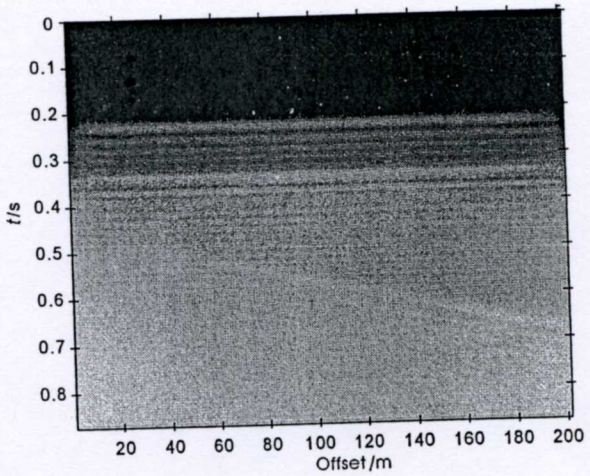

Fig. 10 Seismogram by finite difference as noise level equaling to 0.01

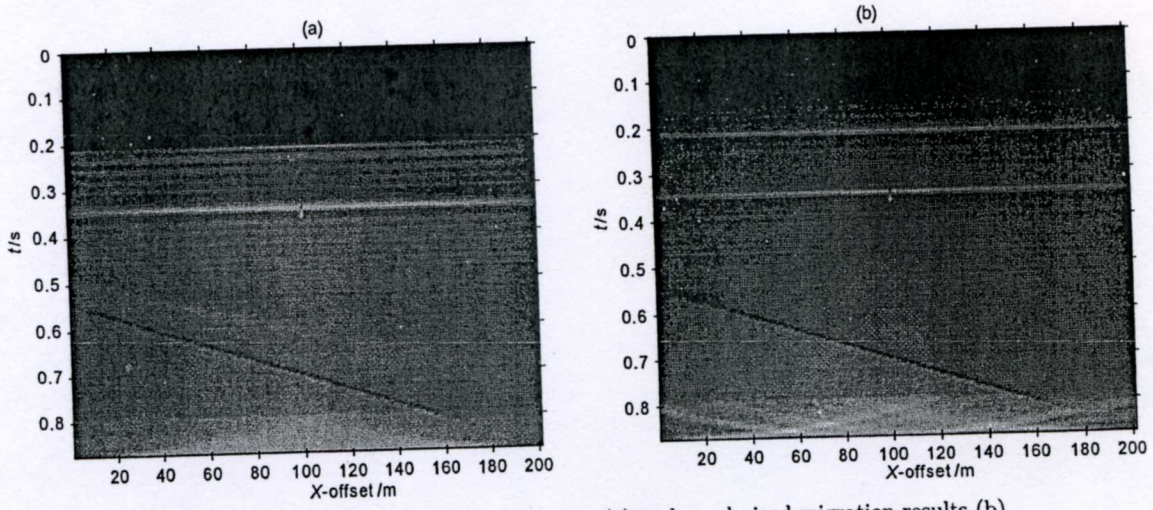

Fig. 11 Standard Kirchhoff migration results (a) and regularized migration results (b)

7 DISCUSSION AND CONCLUSION

Kirchhoff migration is widely used in past decades. However, with the development of the computer and computational techniques, higher quality migration imaging is spot on schedule. This paper addresses the regularized migration deconvolution and inversion issues and proposes a hybrid conjugate gradient method. However, the computational cost of the proposed method is still large. How to accelerating the convergence

of the gradient method while keeping the stability deserves further investigation. In addition, we choose the regularization parameter in an a priori way. According to regularization theory, posteriori choice techniques yield better results. This may be an interesting topic to be studied. Through synthetic simulation, it reveales that regularized migration deconvolution and inversion generates better results than standard migration (as it ought to be). This supplies promising prospect for future extensive usage of the method.

ACKNOWLEDGMENTS

We thank reviewers' helpful comments on the paper. This work is supported by National Natural Science Foundation of China (10871191) and National "973" Key Basic Research Developments Program of China (2005CB422104).

REFERENCES

[1] Aki K, ichards P G. Quantitative Seismology: Theory and Methods. San Francisco: W. H. Freeman and Company, 1980

[2] Claerbout J F. Imaging the Earth's Interior. Oxford: Blackwell, 1985

[3] SjØberg T, Gelius L-J, Lecomte I. 2D deconvolution of seismic image blur. Expanded Abstracts, SEG 73nd Annual Meeting, Dallas, 2003

[4] Nemeth T, Wu C J, Schuster G T. Least-squares migration of incomplete reflection data. *Geophysics*, 1999, **64**(1): 208~221

[5] Guitton A. Amplitude and kinematic corrections of migrated images for nonunitary imaging operators. *Geophysics*, 2004, **69**: 1017~1024

[6] Sacchi M D, Wang J, Kuehl H. Regularized migration/inversion: new generation of imaging algorithms. *CSEG Recorder*, 2006, **31**: 54~59

[7] Levenberg K. A method for the solution of certain nonlinear problems in least squares. *Quart. Appl. Math.*, 1944, **2**: 164~166

[8] Marquardt D W. An algorithm for least-squares estimation of nonlinear inequalities. *SIAM J. Appl. Math.*, 1963, **11**: 431~441

[9] Zeng R, Liu H, Cheng S J, et al. Application of Cauchy-constraint blind deconvolution in cross-hole seismic data processing. *Chinese J. Geophys.* (in Chinese), 2004, **19**: 166~172

[10] Wang Y F. A restarted conjugate gradient method for ill-posed problems. *Acta Mathematicae Applicatae Sinica*, 2003, **19**: 31~40

[11] Wang Y F, Yuan Y X. Convergence and regularity of trust region methods for nonlinear ill-posed inverse problems. *Inverse Problems*, 2005, **21**: 821~838

[12] Tarantola A. Inverse Problems Theory: Methods for Data Fitting and Model Parameter Estimation. Amsterdam: Elsevier, 1987

[13] Yang W C. Geophysical Inversion and Seismic Tomography (in Chinese). Beijing: Geological Publishing House, 1989

[14] Ulrych T J, Sacchi M D, Woodbury A. A Bayesian tour to inversion. *Geophysics*, 2000, **66**: 55~69

[15] Zhang H B, Yang C C. A constrained impedance inversion method controlled by regularized parameters. *Chinese J. Geophys.* (in Chinese), 2003, **46**: 827~834

[16] Wang Y F, Yang C C, Li X W. A regularizing kernel-based brdf model inversion method for ill-posed land surface parameter retrieval using smoothness constraint. *Journal of Geophysical Research*, 2008, **113**, D13101

[17] Lanczos C. Linear Differential Operators. New York: Van Nostrand, 1961

[18] Trampert J, Leveque J J. Simultaneous iterative reconstruction technique: physical interpretation based on the generalized least squares solution. *Journal of Geophysical Research*, 1990, **95**: 12553~12559

[19] Nolet G. Solving or resolving inadequate noisy tomographic systems. *J. Comp. Phys.*, 1985, **61**: 463~482

[20] Nolet G, Snieder R. Solving large linear inverse problems by projection. *Geophys. J. Int.*, 1990, **103**: 565~568

[21] Murio D A. The Mollification Method and the Numerical Solution of Ill-posed Problems. New York: John Wiley and Sons, 1993

[22] Backus G, Gilbert J. Numerical applications of a formalism for geophysical inverse problems. *Geophys. J. R. Astron. Soc.*, 1967, **13**: 247∼276
[23] Backus G, Gilbert J. The resolving power of gross earth data. *Geophys. J. R. Astron. Soc.*, 1968, **16**: 169∼205
[24] Van Decar J C, Snieder R. Obtaining smooth solutions to large linear inverse problems. *Geophysics*, 1994, **59**: 818∼829
[25] Wang Y F. Computational Methods for Inverse Problems and Their Applications (in Chinese). Beijing: Higher Education Press, 2007
[26] Engl H W, Hanke M, Neubauer A. Regularization of Inverse Problems. Dorcrecht: Kluwer Academic Publishers, 1996
[27] Schuster G T, Hu J X. Green's function for migration: Continuous recording geometry. *Geophysics*, 2000, **65**(1): 167∼175
[28] Lecomte I. Resolution and illumination analyses in PSDM: a ray-based approach. *The Leading Edge*, 2008, **27**: 650∼663
[29] Tikhonov A N, Arsenin V Y. Solutions of Ill-posed Problems. New York: John Wiley and Sons, 1977
[30] Xiao T Y, Yu S G, Wang Y F. Numerical Methods for the Solution of Inverse Problems (in Chinese). Beijing: Science Press, 2003
[31] Nashed M Z. Perturbations and approximations for generalized inverses and linear operators equations. In: Nashed M Z ed. Generalized Inverses and Applications, 1976. 325∼396
[32] Schuster G T. Green's functions for migration. Abstracts of Expanded Abstracts 67th SEG meeting, 1997. 1754∼1758
[33] Stolt R H, Benson A K. Seismic Migration: Theory and Practice, Vol. 5, Handbook of Geophysical Exploration, Section I. Seismic Exploration. London: Geophysical Press, 1986
[34] Yilmaz O. Seismic Data Processing, Investigations in Geophysics No. 2. Society of Exploration Geophysicists, Tulsa, Okla, 1987
[35] Hu J X, Schuster G T, Valasek P A. Poststack migration deconvolution. *Geophysics*, 2001, **66**(3): 939∼952
[36] Chen J, Schuster G T. Resolution limits of migrated images. *Geophysics*, 1999, **64**(4): 1046∼1053
[37] Yu J H, Hu J X, Schuster G T, Estill R. Prestack migration deconvolution. *Geophysics*, 2006, **71**(2): S53∼S62
[38] Yuan Y X. Numerical Methods for Nonlinear Programming (in Chinese). Shanghai: Shanghai Science and Technology Publisher, 1993
[39] Touati-Ahmed D, Storey C. Efficient hybrid conjugate gradient techniques. *J. Optimization Theory Appl.*, 1990, **64**: 379∼397